Lead-Free Nanogenerator Made from Single $ZnSnO_3$ Microbelt

Jyh Ming Wu,[†,‡] Chen Xu,[‡] Yan Zhang,[‡] and Zhong Lin Wang[‡,*]

[†]Department of Materials Science and Engineering, Feng Chia University, Taichung 40724, Taiwan, Republic of China and [‡]School of Materials Science and Engineering, Georgia Institute of Technology, Atlanta, Georgia 30332, United States

ABSTRACT

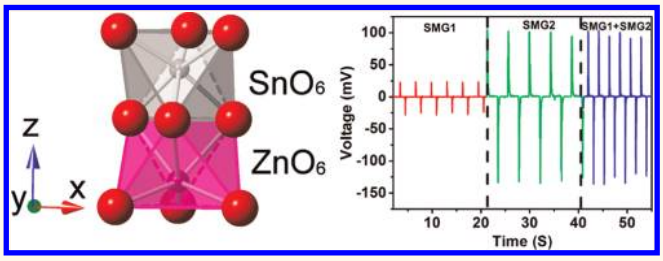

We demonstrated a single-microbelt nanogenerator first made using a $ZnSnO_3$ microbelt that generated an output power of ~3 nW under a compressive and releasing strain of 0.8−1%. The $ZnSnO_3$ nanobelts/microbelts were synthesized using a vapor transfer process at 1173 K. The X-ray diffraction pattern shows that the microbelts belong to $ZnSnO_3$ with rhombohedral structure. An individual $ZnSnO_3$ microbelt was bonded at its ends on a flexible polystyrene substrate as a nanogenerator, which gives an output voltage and current of 100 mV and 30 nA, respectively, corresponding to an energy conversion efficiency of 4.2−6.6% (based on 0.8−1% strain). Our results show that $ZnSnO_3$ microbelts are one of the highly promising materials for lead-free piezoelectric energy harvesting.

KEYWORDS: $ZnSnO_3$ · microbelts · lead-free · piezoelectric nanogenerator

Non-centrosymmetric (NCS) oxides[1] have attracted considerable attention due to their unique symmetry-dependent and spontaneous polarization properties, which are technologically important and are the basis of numerous applications in ferroelectricity, piezoelectricity, and nonlinear optics.[2] Among NCS oxides, ZnO is an environmentally friendly and piezoelectric material.[3] Therefore, single ZnO nanowires/microwires have extensively been demonstrated as piezoelectric diodes,[4] piezotronic transistors,[5] nanogenerators,[6] solar cells,[7] and strain sensors.[8]

Besides ZnO, there are still many lead-free piezoelectric materials in the NCS group that remain to be undiscovered, especially in terms of perovskite structure. Despite the success in lead-based piezoelectric materials (*i.e.*, lead zirconate titanate) due to their high polarization and piezoelectric performance as transducers,[9] a consistent effort has been taken to replace Pb-based materials with some as yet undiscovered lead-free materials[10] that would be more environmentally friendly and enable new piezoelectric applications for mechanical energy harvesting.[11] Recently, Inaguma[2] reported a lead-free $LiNbO_3$ (LN)-type $ZnSnO_3$ using a high-pressure (~7 GPa) synthesized environment. Son *et al.*[12] reported that the epitaxial (111) $ZnSnO_3$ thin film exhibited a highly ferroelectric polarization of ~47 μCcm^{-2} using a pulsed laser deposition process. In NCS oxides, $ZnSnO_3$ is primarily characterized by a large displacement of Zn based on a strong covalent bond between three oxygen and zinc atoms, resulting in the $ZnSnO_3$ having a strong piezoelectric response. Therefore, $ZnSnO_3$ has also attracted a lot of attention recently.[13,14] However, most works focused on the structural characterization[15] and theoretical calculation[14,16] of polarization, especially in thin film and bulk materials of $ZnSnO_3$.[17] There is no complete report regarding crystallographic and energy harvesting using $ZnSnO_3$ nanostructures. Therefore, the synthesis route, structural analysis, and energy harvesting application of $ZnSnO_3$ nanostructures still remain unclear and are subject to a comprehensive investigation.

In particular, the synthesis of the LN-type $ZnSnO_3$ is a challenge due to the extreme conditions of high pressure.[18] In this work, we report that $ZnSnO_3$ nanobelts/microbelts can be successfully grown through a carbon-thermal reaction process at a temperature of 1173 K. On the basis of X-ray diffraction characterization, two major peaks of (110) and (104) appear in the spectrum of $ZnSnO_3$ nanobelts, indicating that the $ZnSnO_3$ nanostructures have a rhombohedral structure. Although there still exist several second phases in our products, this is the first case in which the

* Address correspondence to zlwang@gatech.edu.

Received for review March 2, 2012 and accepted April 6, 2012.

Published online 10.1021/nn300951d

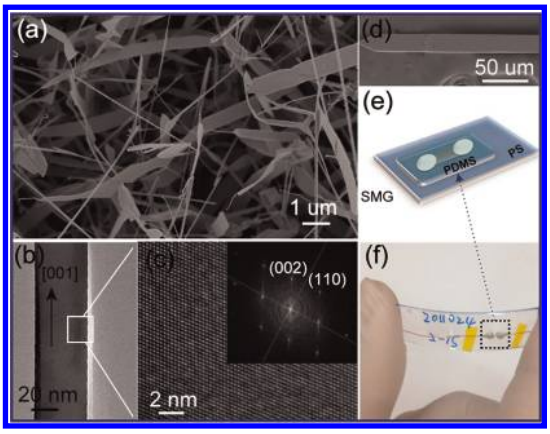

Figure 1. Structure characterization of $ZnSnO_3$ belts. (a) Field emission microscopy image of $ZnSnO_3$ nanobelts. (b) Individual $ZnSnO_3$ microbelts obviously exhibited trigonal prism morphology. (c) Corresponding high-resolution transmission electron microscopy image and fast Fourier transform (FFT) pattern (inset of c) show that the nanobelt grows along the [001] direction. (d) SEM image of an individual $ZnSnO_3$ microbelt. (e) Schematic diagram of a single microbelt nanogenerator (SMG). (f) Photograph of a SMG.

$ZnSnO_3$ nanobelts/microbelts were available for piezoelectric energy harvesting. Furthermore, an individual microbelt was carefully manipulated for fabricating a single microbelt nanogenerator (SMG) to investigate the output power and piezoelectric performance of $ZnSnO_3$. Through our detailed investigations, the SMG can produce a voltage and current of 100 mV and 30 nA, respectively. The energy conversion efficiency of a single SMG can reach 6.6% under an applied 0.8% compressive strain. With the integration of two SMGs in parallel and serial connection, the voltage and current can exceed 110 mV and 80 nA, respectively. This discovery revealed a useful, alternative lead-free nanomaterial for piezoelectricity and energy harvesting.

RESULTS AND DISCUSSION

The nanostructure of the as-synthesized material was first investigated. Figure 1a shows that the $ZnSnO_3$ were formed as belt-like nanostructures after a carbon-thermal reaction at 1173 K. The dimension of the belt-like $ZnSnO_3$ nanostructures was less than 100 nm in thickness and up to 1000 μm in length. Transmission electron microscopy (TEM) analysis of an individual nanobelt is shown in Figure 1b. High-resolution TEM image and corresponding fast Fourier transform (FFT) pattern are shown in Figure 1c and its inset, in which the FFT pattern corresponds to the diffraction spot of the (110) plane, which is one of the major planes in the $ZnSnO_3$ phase. The growth direction was governed by the [001] axis, confirming that the spontaneous polarization direction is along the *z*-axis. To further demonstrate that the crystal nanostructures belong to the $ZnSnO_3$, the X-ray diffraction (XRD) pattern (see Supporting Information in Figure S1) shows two major peaks of (104) and (110), indicating that the as-synthesized nanobelts are attributed to the major phase of $ZnSnO_3$ (JCPDS 52-1381) with a lattice constant of $a = b = 0.52622$ nm, $c = 1.40026$ nm. The second major phase is still Zn_2SnO_4,[19] which belongs to a spinel structure and exhibited pseudoperiodically twin-structure morphology (see Figure S2 in the Supporting Information).[20] The $ZnSnO_3$ microbelts can be easily recognized for the fabrication of a nanogenerator, even though there are still several residual second phases in the as-synthesized products.

To simplify the manipulation of a single microbelt during the fabrication of a SMG, the synthesized time was increased to enlarge the dimension of the nanobelts. The dimension of $ZnSnO_3$ nanobelts can therefore reach lengths of up to 1500 μm; the nanobelts' width and thickness were also obviously increased. Figure 1d shows that an individual microbelt was formed by trigonal-pyramidal morphology. In the design of the SMG, a microbelt was carefully manipulated to lie on a flexible polystyrene (PS) substrate (length $\times$ width $\times$ thickness $\approx$ 40 $\times$ 10 $\times$ 1 mm) and fixed to electrodes at both ends, as shown in Figure 1e. Figure 1f is a photograph showing that the SMG was fixed on a PS substrate covered by a thin layer of PDMS, and a mechanically compressive force was applied on both sides. When the substrate was bent with a cyclical compressive force, a compressive strain $\varepsilon = 0.8-1\%$ was created in the microbelt. The calculated method of the substrate's strain is shown in Supporting Information S1.[8,21]

The atomic structure of $ZnSnO_3$ is presented using octahedral units, as shown in Figure 2a. Each Zn octahedron shares corners with another Zn octahedron, and each Sn octahedron shares corners with another Sn octahedral structure. The cation sequence is Sn−Zn−vacancy−Sn−Zn−vacancy (see Figure 1, top to bottom) and is aligned along the *z*-axis, as seen in Figure 2a. Figure 2b further displays two octahedral frameworks of ZnO_6 (lower side) and SnO_6 (upper side). The octahedral SnO_6 and ZnO_6 share both edges and faces with the adjacent octahedra. Figure 2c indicates the single cluster of ZnO_6 and SnO_6. The bonding lengths of Zn−O, as labeled by l_a and l_b in the ZnO_6 cluster, have three long bonds of ~0.2308 nm at the upper side and three short bonds of ~0.2040 nm at the lower side, respectively. In contrast, the bonding lengths of the Sn−O, as labeled by l_c and l_d in the SnO_6 cluster, have three short bonds of ~0.2008 nm at the upper side and three long bonds of ~0.2093 nm at the lower side, respectively. To evaluate how much deviation of bonding length existed in O−Zn−O and O−Sn−O bonds along the *z*-axis in a single ZnO_6 and a single SnO_6 cluster, respectively, the single clusters of ZnO_6 and of SnO_6 are further shown in Figure 2d. We concluded that the displacement of the Zn ion (δ_{Zn}) in the ZnO_6 cluster is 0.5 Å, while that of the Sn ion (δ_{Sn}) in the SnO_6 cluster is 0.2 Å. The displacement in the Zn ion

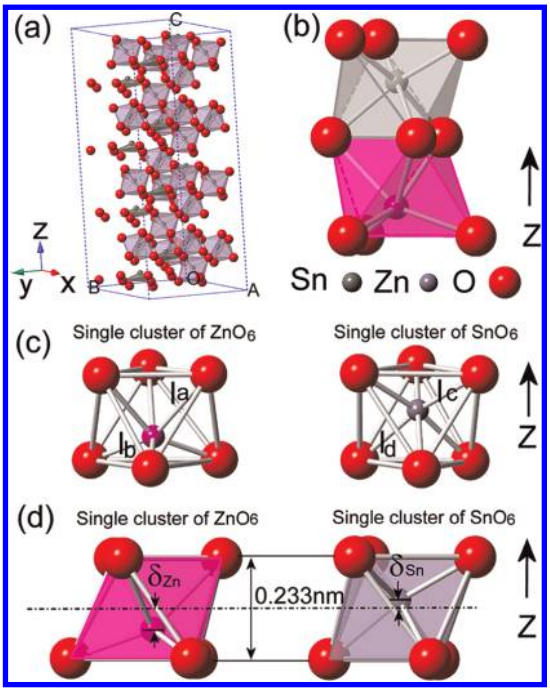

Figure 2. Crystallographic structure of $ZnSnO_3$. (a) Three-dimensional image shows the crystal structure of $ZnSnO_3$ from the perspective of an octahedral framework. The cation sequence is Sn−Zn−vacancy−Sn−Zn−vacancy along the *z*-axis. (b) Two octahedral frameworks of ZnO_6 (lower side) and SnO_6 (upper side). (c) Individual single cluster of ZnO_6 shows three long bonds (upper side) and short bonds (lower side) of l_a and l_b, respectively. In contrast, SnO_6 shows three short bonds (upper side) and long bonds (lower side) of l_c and l_d, respectively. (d) The deviation of Zn (δ_{zn}) and Sn (δ_{Sn}) ions in the bonding length of O−Zn−O and O−Sn−O along the *z*-axis, respectively.

is greater than that of the Sn ion along the *z*-axis. Therefore, a spontaneous polarization is generated along the *z*-axis, which is the source of piezoelectricity in this material. The unit cell used for calculating the crystal structure was carried out using space group *R*3*c*, as listed in the Supporting Information, Table S1.

Electrical measurement showed that both SMGs exhibited Schottky behavior at one end in Figure 3a. The output voltage of a single nanogenerator for SMG no. 1 and no. 2 can reach 25 and 100 mV, respectively (see Figure 3b, SMG1 and SMG2). The output current of SMG no. 1 and no. 2 can exceed 50 and 30 nA, respectively (see Figure 3c, SMG1 and SMG2). By integrating two SMGs in serial connection, the output voltage can exceed 110 mV (see Figure 3b, blue-colored line, SMG1 + SMG2). The output current of SMG no. 1 and SMG no.2 in parallel connection can reach 80 nA (see Figure 3c, blue-colored line).

The piezopotential distribution in a single microbelt was investigated under applied compressive strain. For simplicity, the piezopotential was calculated without considering the carrier concentration.[22,23] The material constants of $ZnSnO_3$ used for the calculation were elastic constants: C_{11} = 194 GPa, C_{12} = 63 GPa, C_{13} = 101 GPa, C_{15} = 0.1 GPa, C_{33} = 169 GPa, C_{44} = 117 GPa, and C_{66} = 92 GPa. The piezoelectric stress constants for e_{11}, e_{15}, e_{31}, and e_{33} are −0.15, 0.26, 1.23, and 0.29 C m^{-2}, respectively.[24] Figure 4a shows that, when the microbelt was subjected to a compressive strain along the *z*-direction, the polarization of atoms generated an ionic charge and resulted in a piezopotential change from V^- to V^+, namely, the generation of a piezoelectric field along the microbelt in the *z*-direction. Therefore, the calculated piezopotential at the end of the $ZnSnO_3$ microbelts is up to 196 V, demonstrating that the $ZnSnO_3$ possesses high piezopotential performance in the lead-free piezoelectric material system. However, the actual piezopotential in $ZnSnO_3$ microbelts is much lower than the calculated value, owing to the screening effect of the free charge carriers and the finite conductance.[25,26] This fact explains how the low conductance SMG no. 1 exhibited a higher output current, while the high conductance SMG no. 2 showed a lower output current due to the free carriers' effect in the microbelts. On the basis of our previous work,[12] the output voltage can be ascribed to the size effect. In this case, the SMG no. 1 and no. 2 have almost the same dimension; thus the size effect was omitted.

Figure 4b (see red-colored line) shows a typical Shottky barrier ($\sim\Phi_{SB}$) of SMG in an original state. When the SMG was subjected to a compressive strain, the generated piezopotential, which is positive (V^+) at the Schottky barrier (Φ_{SB}) side and negative (V^-) at the ohmic contact side, creates an instantaneous difference in Fermi levels of $\sim\delta_{Ep}$ (see Figure 4c). Because the resistance of the Schottky barrier existence blocks the diffusion of electrons through the microbelt, the electrons will flow from the left electrode to the right electrode through an external load. The electrons first accumulate at the interfacial region between the right electrode and microbelt; the process continues until the potential generated by piling up the electrons balances the difference in Fermi levels (δ_{Ep}). When the compressive strain is instantly released in the SMG, the disappearance of the piezoelectric potential results in a lower Fermi level of the left electrode for δ_{Ep} (see the blue, dashed line in Figure 4d). The electrons accumulated near the right electrode flow back through the external circuit to the left electrode, recovering the SMG to its initial stage.

To investigate the energy conversion efficiency of the SMG, the following eq 1 was used to determine the amount of strain energy (U_m) that was stored in the microbelt:[4]

$$U_m = \frac{1}{2} E A L_0 \varepsilon_{zz}^2 \qquad (1)$$

where ε_{zz} is the strain along the *z*-axis.[8] The shear strain can be omitted owing to the compressive radius *R* of the substrate, which is much larger than that of the length of the microbelt. *E* is Young's modulus of $ZnSnO_3$ (~238 GPa),[16] *A* is the cross-sectional area of a single microbelt, and L_0 is the original length of the

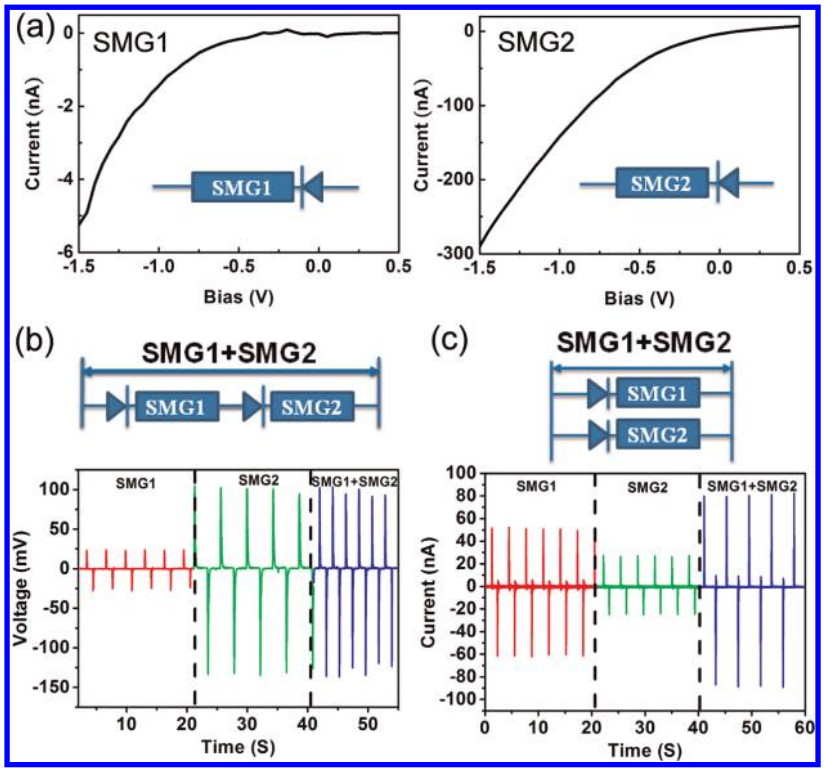

Figure 3. (a) $I-V$ characteristic of a SMG, showing a typical Schottky diode characteristic. (b) Electrical output voltage with serial connection of SMG no. 1 and SMG no. 2 (c) Electrical output current with parallel connection of SMG no. 1 and SMG no. 2.

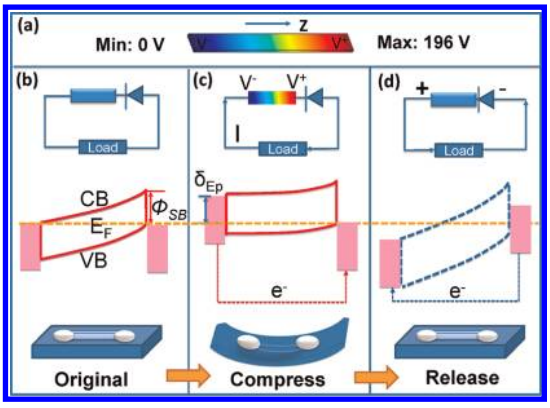

Figure 4. (a) Theoretical calculation of piezoelectric potential in a compressive strain of a single $ZnSnO_3$ microbelt. (b) SMG at the original state, a Schottky contact with a metal electrode on the right and an ohmic contact with an electrode on the left, Φ_{SB} is the Schottky barrier height. (c) SMG at the compressive state. (d) SMG at the released state (see details in text). δ_{Ep} is the difference in Fermi Level between the two electrodes in the presence of piezoelectric potential. The dotted, orange-colored line is the original Fermi level E_F; CB and VB are the conduction and valence bands of the $ZnSnO_3$, respectively.

microbelt. To evaluate the total energy conversion efficiency, the electric energy generation can be calculated by eq 2. U_e is the electrical output energy:

$$U_e = \int IV dt \qquad (2)$$

where I and V are the output current and voltage of the SMG, respectively (see Supporting Information, Figure S3). Thus, the U_m and U_e are 5.52×10^{-7} and 3.65×10^{-8} J, respectively. Therefore, the conversion efficiency (U_e/U_m) of SMG is 6.6% (the length, width, and thickness of the microbelt are $\sim 477 \times 19 \times 8\ \mu$m, respectively, with a compressive strain of ~0.8%; see Supporting Information, Figure S4), which is comparable to that of a ZnO wire in our previous study.[6] Figure 5 shows that the output voltage of SMGs in parallel connection were not affected significantly by increasing the driving frequency from 0.33 to 1.2 Hz, which shows that the output voltage exhibited high stability, demonstrating that the SMG made from $ZnSnO_3$ microbelts is very suitable for energy harvesting driven by irregular excitations in our living environment.

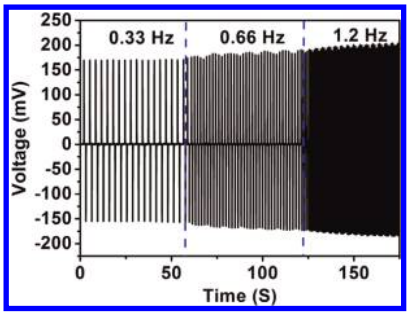

Figure 5. The SMG shows good stability with an increase in driving frequency.

CONCLUSION

In summary, $ZnSnO_3$ nanobelts/microbelts were successfully synthesized using a vapor transfer process.

Individual $ZnSnO_3$ microbelts were applied for piezoelectric energy conversion for the first time. The SMGs can produce an output voltage and current exceeding 110 mV in parallel connection and 80 nA in serial connection, respectively. The total energy conversion efficiency can reach 6.6% based on the microbelt dimensions of ~477 × 19 × 8 μm with 0.8% strain. This study demonstrates the possibility of using the lead-free piezoelectric material of $ZnSnO_3$ microbelts for energy conversion.

EXPERIMENTAL METHOD

Material Synthesis. A Zn−Sn buffer layer was predeposited on Si and alumina substrates to act as a seed layer. The source materials of Zn and Sn (0.5 g, purity: 99.9%) were separately placed on an alumina boat with a length of 5 cm, and relative source materials with 50 wt % of graphite powder were positioned in the center zone of a quartz reactor to conduct the carbon-thermal reaction with an annealing process. The reaction took place at a constant temperature of 1173 K and was maintained at 10−20 Torr for 3 h. The gas flow rates of argon and oxygen were 200 sccm and 10−20 sccm, respectively (O_2, purity: 99.9%). To simplify the manipulation, ultralong $ZnSnO_3$ microbelts of ~300−1000 μm were used for fabricating the SMGs. A $ZnSnO_3$ microbelt was placed on a polystyrene substrate 40 mm in length, 10 mm in width, and 1 mm in thickness. Each microbelt was fixed to the substrate using silver paste; metal wires were bonded to the end of each microbelt for power measurement. An additional layer of polydimethylsiloxane (PDMS) was used to package the SMG device to keep the SMG device robust under the period of cyclical mechanical deformation and manipulation.

Electrical Measurement. The SMGs' measurement method is the same as in our prior study.[27] The output signal of the nanogenerator was measured by using a low-noise voltage preamplifier (Stanford Research System model SR560) and a low-noise current preamplifier (Stanford Research System model SR570).

Conflict of Interest: The authors declare no competing financial interest.

Acknowledgment. The authors would like to thank the support from National Science Council of the Republic of China (100-2918-I-035-003 and NSC 100-2628-E-035-006-MY2), BES DOE, and NSF.

Supporting Information Available: (1) X-ray diffraction pattern, (2) optical microscopy and TEM image, (3) structural parameters of $ZnSnO_3$, (4) output current and voltage of the SMG no. 2, and (5) substrate strain calculation method. This material is available free of charge *via* the Internet at http://pubs.acs.org.

REFERENCES AND NOTES

1. Halasyamani, P. S.; Poeppelmeier, K. R. Noncentrosymmetric Oxides. *Chem. Mater.* **1998**, *10*, 2753–2769.
2. Inaguma, Y.; Yoshida, M.; Katsumata, T. A Polar Oxide $ZnSnO_3$ with a $LiNbO_3$-Type Structure. *J. Am. Chem. Soc.* **2008**, *130*, 6704–6705.
3. Wang, Z. L.; Song, J. H. Piezoelectric Nanogenerators Based on Zinc Oxide Nanowire Arrays. *Science* **2006**, *312*, 242–246.
4. Yang, Q.; Wang, W. H.; Xu, S.; Wang, Z. L. Enhancing Light Emission of ZnO Microwire-Based Diodes by Piezo-Phototronic Effect. *Nano Lett.* **2011**, *11*, 4012–4017.
5. Wang, X. D.; Zhou, J.; Song, J. H.; Liu, J.; Xu, N. S.; Wang, Z. L. Piezoelectric Field Effect Transistor and Nanoforce Sensor Based on a Single ZnO Nanowire. *Nano Lett.* **2006**, *6*, 2768–2772.
6. Yang, R. S.; Qin, Y.; Dai, L. M.; Wang, Z. L. Power Generation with Laterally Packaged Piezoelectric Fine Wires. *Nat. Nanotechnol.* **2009**, *4*, 34–39.
7. Yang, Y.; Guo, W. X.; Zhang, Y.; Ding, Y.; Wang, X.; Wang, Z. L. Piezotronic Effect on the Output Voltage of P3HT/ZnO Micro/Nanowire Heterojunction Solar Cells. *Nano Lett.* **2011**, *11*, 4812–4817.
8. Zhou, J.; Gu, Y. D.; Fei, P.; Mai, W. J.; Gao, Y. F.; Yang, R. S.; Bao, G.; Wang, Z. L. Flexible Piezotronic Strain Sensor. *Nano Lett.* **2008**, *8*, 3035–3040.
9. Kingon, A. I.; Srinivasan, S. Lead Zirconate Titanate Thin Films Directly on Copper Electrodes for Ferroelectric, Dielectric and Piezoelectric Applications. *Nat. Mater.* **2005**, *4*, 233–237.
10. Zeches, R. J.; Rossell, M. D.; Zhang, J. X.; Hatt, A. J.; He, Q.; Yang, C. H.; Kumar, A.; Wang, C. H.; Melville, A.; Adamo; *et al.* A Strain-Driven Morphotropic Phase Boundary in $BiFeO_3$. *Science* **2009**, *326*, 977–980.
11. Jung, J. H.; Lee, M.; Hong, J. I.; Ding, Y.; Chen, C. Y.; Chou, L. J.; Wang, Z. L. Lead-Free $NaNbO_3$ Nanowires for a High Output Piezoelectric Nanogenerator. *ACS Nano* **2011**, *5*, 10041–10046.
12. Son, J. Y.; Lee, G.; Jo, M. H.; Kim, H.; Jang, H. M.; Shin, Y. H. Heteroepitaxial Ferroelectric $ZnSnO_3$ Thin Film. *J. Am. Chem. Soc.* **2009**, *131*, 8386–8387.
13. Nakayama, M.; Nogami, M.; Yoshida, M.; Katsumata, T.; Inaguma, Y. First-Principles Studies on Novel Polar Oxide $ZnSnO_3$, Pressure-Induced Phase Transition and Electric Properties. *Adv. Mater.* **2010**, *22*, 2579–2582.
14. Zhang, J.; Yao, K. L.; Liu, Z. L.; Gao, G. Y.; Sun, Z. Y.; Fan, S. W. First-Principles Study of the Ferroelectric and Nonlinear Optical Properties of the $LiNbO_3$-Type $ZnSnO_3$. *Phys. Chem. Chem. Phys.* **2010**, *12*, 9197–9204.
15. Mizoguchi, H.; Woodward, P. M. Electronic Structure Studies of Main Group Oxides Possessing Edge-Sharing Octahedra: Implications for the Design of Transparent Conducting Oxides. *Chem. Mater.* **2004**, *16*, 5233–5248.
16. Ge, N. N.; Liu, C. M.; Cheng, Y.; Chen, X. R.; Ji, G. F. First-Principles Calculations for Elastic and Electronic Properties of $ZnSnO_3$ Under Pressure. *Phys, B: Condens. Matter* **2011**, *406*, 742–748.
17. Wang, H.; Huang, H. T.; Wang, B. A. First-Principles Study of Structural, Electronic, and Optical Properties of $ZnSnO_3$. *Solid State Commun.* **2009**, *149*, 1849–1852.
18. Hoel, C. A.; Amores, J. M. G.; Moran, E.; Alario-Franco, M. A.; Gaillard, J. F.; Poeppelmeier, K. R. High-Pressure Synthesis and Local Structure of Corundum-Type $In_{2-2x}Zn_xSn_xO_3$ ($x \leq 0.7$). *J. Am. Chem. Soc.* **2010**, *132*, 16479–16487.
19. Gracia, L.; Beltran, A.; Andres, J. A Theoretical Study on the Pressure-Induced Phase Transitions in the Inverse Spinel Structure Zn_2SnO_4. *J. Phys. Chem. C* **2011**, *115*, 7740–7746.
20. Chen, H. Y.; Wang, J. X.; Yu, H. C.; Yang, H. X.; Xie, S. S.; Li, J. Q. Transmission Electron Microscopy Study of Pseudoperiodically Twinned Zn_2SnO_4 Nanowires. *J. Phys. Chem. B* **2005**, *109*, 2573–2577.
21. Zhou, J.; Fei, P.; Gu, Y. D.; Mai, W. J.; Gao, Y. F.; Yang, R.; Bao, G.; Wang, Z. L. Piezoelectric-Potential-Control led Polarity-Reversible Schottky Diodes and Switches of ZnO Wires. *Nano Lett.* **2008**, *8*, 3973–3977.
22. Gao, Y.; Wang, Z. L. Equilibrium Potential of Free Charge Carriers in a Bent Piezoelectric Semiconductive Nanowire. *Nano Lett.* **2009**, *9*, 1103–1110.
23. Mantini, G.; Gao, Y. F.; D'Amico, A.; Falconi, C.; Wang, Z. L. Equilibrium Piezoelectric Potential Distribution in a Deformed ZnO Nanowire. *Nano Res.* **2009**, *2*, 624–629.
24. Zhang, J.; Xu, B.; Qin, Z.; Li, X. F.; Yao, K. L. Ferroelectric and Nonlinear Optical Properties of The $LiNbO_3$-Type $ZnGeO_3$ from First-Principles Study. *J. Alloys Compd.* **2012**, *514*, 113–119.
25. Shao, Z. Z.; Wen, L. Y.; Wu, D. M.; Zhang, X. A.; Chang, S. L.; Qin, S. Q. Influence of Carrier Concentration on

Piezoelectric Potential in a Bent ZnO Nanorod. *J. Appl. Phys.* **2010**, *108*.
26. Zhang, Y.; Liu, Y.; Wang, Z. L. Fundamental Theory of Piezotronics. *Adv. Mater.* **2011**, *23*, 3004–3013.
27. Hu, Y. F.; Lin, L.; Zhang, Y.; Wang, Z. L. Replacing a Battery by a Nanogenerator with 20 V Output. *Adv. Mater.* **2012**, *24*, 110–114.